Eur. Phys. J. Spec. Top.
https://doi.org/10.1140/epjs/s11734-024-01402-0

THE EUROPEAN PHYSICAL JOURNAL SPECIAL TOPICS

Regular Article

In-line monitoring of a multi-stage drying process for battery electrodes: vol. 1—applying methods of scattered light measurement

Jonas Mohacsi[1,2,a], Kevin Ly[1,2,b], Marius Birg[1], Philip Scharfer[1,2,c], and Wilhelm Schabel[1,2,d]

[1] Thin Film Technology, Karlsruhe Institute of Technology, Kaiserstraße 12, Karlsruhe 76131, Germany
[2] Material Research Center for Energy Systems (MZE), Karlsruhe Institute of Technology, Kaiserstraße 12, Karlsruhe 76131, Germany

Received 14 May 2024 / Accepted 8 November 2024

Abstract The drying process of battery electrodes is a crucial and expensive step in the battery manufacturing process as it significantly impacts the performance of the final cell. One major challenge is minimising high scrap rates, which has a marked impact on material efficiency and production costs. One approach is to utilise additional in-line sensors to detect and prevent defects at an early stage. Established sensor technology has been employed primarily to measure parameters prior to and subsequent to the drying process. The objective of this study is to examine the potential of a scattered light sensor for monitoring the electrode surface during drying for the first time. The sensor's ability to detect surface roughness during drying was demonstrated in initial experiments. Further extensive investigations successfully determined the characteristic point of the onset of pore emptying by the sensor. The results suggest that in-line deployment of the scattered light sensor can be highly beneficial, particularly for multi-stage drying processes. On one hand, the sensor serves as a tool for the straightforward configuration of a multi-stage drying process, and on the other hand, for the in-line utilisation of the sensor with the aim of quality assurance.

1 Introduction

The growing demand for energy storage positions batteries as one of the main players in the process of the energy transition. As the electrification of the transport sector and digitalisation continue to advance, the production of battery cells is set to increase significantly. The drying process of battery electrodes represents one of the most challenging, sensitive, and costly steps in battery manufacturing, playing a key role in determining the quality of the final cell [1]. Presently, the cell production industry faces significant scrap rates of 5–30 % of the total cell production [2][3][4], posing substantial implications for costs, material efficiency, and energy efficiency in the production process. In-line measurement technologies to monitor the electrode production are only partially established. Several publications, such as Schnell and Reinhart [5] or Turetskyy et al. [6], have considered quality gate concepts that allow early detection and prevention of production defects. Those approaches require the implementation of comprehensive in-line sensor technology. Therefore, this publication examines the monitoring of the drying process using a scattered light sensor. The application of a scattered light sensor for this purpose represents a novel approach. The sensor enables the characterisation of surface properties of the electrode layer during its drying process through a straightforward measurement principle. This characterisation provides insight into the current state of the drying process by identifying characteristic milestones such as the onset of pore emptying.

[a] e-mail: jonas.mohacsi@kit.edu (corresponding author)
[b] e-mail: kevin.ly@kit.edu
[c] e-mail: philip.scharfer@kit.edu
[d] e-mail: wilhelm.schabel@kit.edu

Published online: 29 November 2024

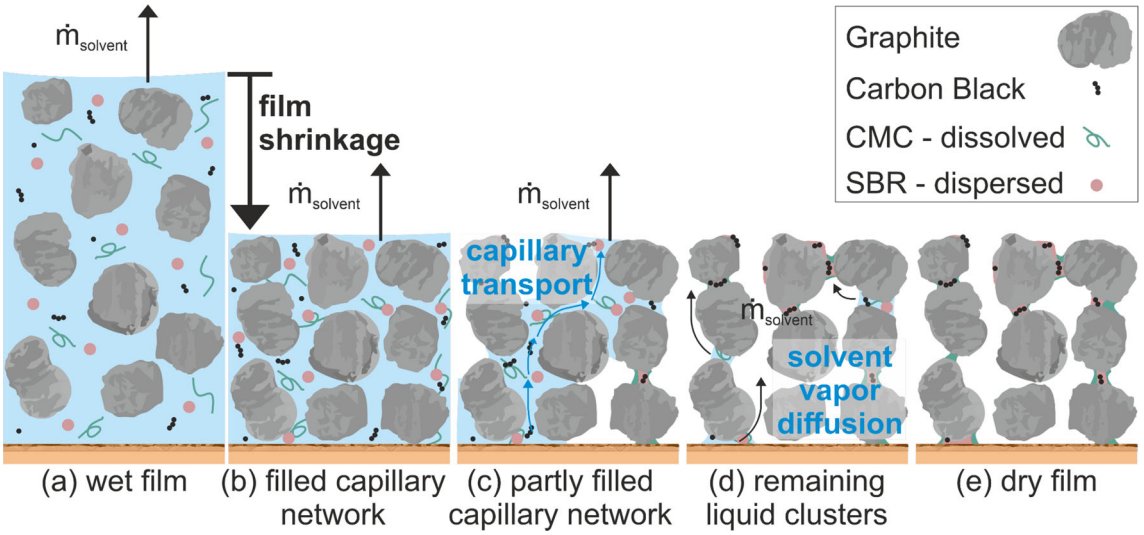

Fig. 1 Schematic illustration delineating the drying process of a graphite anode, progressing through the stages: **a** initial wet film; **b** initial shrinkage of the film controlled by surface solvent evaporation, culminating in the attainment of final film height; **c** after the onset of pore emptying, the pore network empties through the mechanism of capillary transport; **d** when only sporadic, isolated liquid clusters remain, the mechanism of capillary transport ceases. Their evaporation and diffusion to the surface occur within the pore network until the dry film **e** remains [7]. Copyright 2019, Energy Technology

1.1 Microstructure formation during drying process

To comprehend the advantages of this application, it is necessary to understand the mechanisms inside the complex pore network during the drying process of a particulate wet film. The publications by Jaiser et al. [8] and Kumberg et al. [7] have demonstrated that the drying process of battery electrodes follows a schematic representation, as illustrated in Fig. 1. One of the principal constraints on the applicability of drying rates is the mechanism of binder migration. This topic has been extensively explored in multiple publications [9–11]. This process causes the binder, which is initially distributed uniformly within the film, to migrate towards the upper region of the film, resulting in binder accumulation. The absence of binder on the lower film side may result in a decreasing adhesion of the electrode to the substrate foil, which could potentially cause electrode delamination in severe cases. Furthermore, agglomeration of binders may impede ion transport, which significantly reduces cell performance [12–14].

Jaiser et al. [15] observed that capillary forces driving binder migration occur exclusively during a specific phase (b–d) of the drying process. To address this, they proposed a multi-stage drying process with a high drying rate at the beginning (a–b) and end (d–e) of the process, and a significant reduction in the drying rate during the intermediate phase (b–d) [16]. This approach enables a substantial reduction of the drying time without compromising the integrity of the film. Altvater et al. [17] demonstrated that employing a three-stage drying process, facilitated by infrared radiators, can lead to a reduction in drying time of up to 60% without compromising the adhesion strength of the electrode or the cycle stability of the cell. However, the challenge in implementing a multi-stage drying process is to maintain accurate process control, which involves the precise modulation of drying rates at specific intervals. Nevertheless, it is essential that the overall stability of the process is not compromised. To achieve this, the presence of a sensor system that allows the detection of characteristic time points such as the onset of pore emptying and the collapse of the capillary network becomes highly advantageous. Consequently, this study explores the potential of a scattered light sensor for this purpose.

2 Experimental setup

2.1 Slurry preparation

The slurry was prepared applying a dissolver (Dispermat CN10, VMA Gretzmann, Germany). Prior to the actual wet mixing with a CMC solution, a dry mixing step involving graphite and carbon black was carried out for 10 min at 300 rpm. After adding the CMC solution, the wet mixing phase took place for 45 min at 1500 rpm, during which the slurry was simultaneously degassed and cooled. Following this main mixing step, styrene butadiene rubber (SBR) was introduced to the slurry and blended under moderate conditions (10 min at 500 rpm). The composition

Table 1 Dry composition of the anode slurry used in this study

Component	Concentration (dry wt.-%)
Hitachi SMG-A (Graphite)	93
Timcal SuperC65 (Conductive carbon black)	1.4
Carboxy-Methyl-Cellulose "CMC" (Binder, Sunrose MAC500LC, Nippon Paper Industries)	1.87
Styrene-Butadiene Rubber "SBR" (Binder, Zeon Europe GmbH)	3.73

of the dry electrode is summarised in Table 1. The proportion of total solids in the total mass was 43 wt%, with the remainder being demineralised water (57 wt%).

2.2 Coating and drying setup

An extensive description of the doctor blade coating procedure, the dryer ("Comb Nozzle") and the methodology for detecting pore breakthrough using a digital microscope (Keyence, VHX-6000) has already been given in the previous publications of Kumberg et al. [18, 19]. The reader is, therefore, encouraged to consult the referenced paper for further information.

2.3 Multi-stage drying and measurement procedure

The investigation of an optimal timing for adjusting the drying rate in a multi-stage drying process requires the performance of so-called transition drying experiments, as already conducted in the publications of Jaiser et al. [16] and Altvater et al. [17]. In this process, the drying rate is adjusted at a predefined transition time t_{trans} from a high drying rate (HDR) to a low drying rate (LDR). This is achieved by adjusting the distance of the dryer hood to the electrode from 8 to 24 mm as shown in Fig. 2. At the transition time t_{trans}, a measurement is taken with the scattered light sensor (Optosurf OS500), allowing to determine the parameters Aqm and Im. A comprehensive description of the sensor, the measurement principle and specific parameters is provided in Sect. 3. The measurement sequence (B) of the sensor requires a time span of approximately 2–3 s. Following the measurement, drying continues at a low rate until the layer is dry. After completing the drying experiment, the adhesion of the electrode to the substrate foil is measured. The described procedure is repeated multiple times,

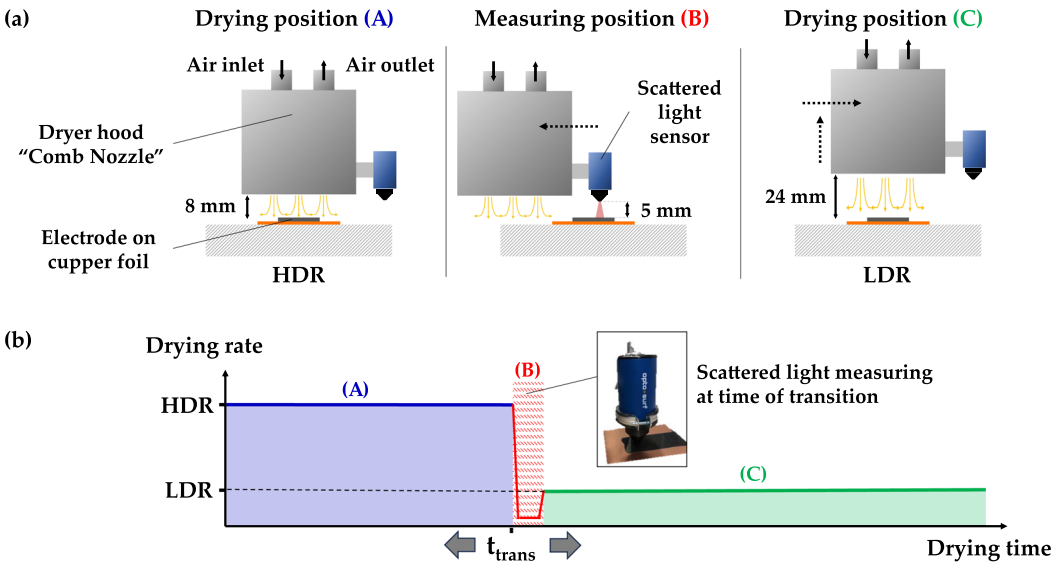

Fig. 2 **a** Setup for drying experiments: "Comb Nozzle" dryer with vertically and horizontally adjustable dryer hood. Vertical height adjustment of the dryer hood for setting the drying rate (Drying position (A) and (C)). Horizontal movement of the dryer hood for sensor measurement (Measuring position (B)). **b** The adjustment of the dryer hood position allows the indicated drying procedure to be carried out: (A) Drying position (8 mm), high drying rate; (B) measurement of scattered light sensor; (C) Drying position (24 mm), low drying rate

varying the transition time (HDR → LDR) at each iteration. Subsequently, plotting the measured adhesion force against the switching time yields the characteristic curves outlined in Sect. 4.

2.4 Adhesion force determination

The adhesion force between the electrodes and the substrate foil was assessed utilising an AMETEK LS1 universal testing machine (Lloyd Instruments Ltd., UK), equipped with a 90° peeling device and a 10 N load cell. Specimens measuring 30 mm in width were subjected to testing, cut perpendicular to the coating direction, with three specimens per electrode. The resulting mean value and standard deviation were calculated.

3 Scattered light measurement

The method of scattered light measurement is already widely employed for quality assurance in industrial manufacturing [20, 21]. However, the application of a scattered light sensor to characterise the drying progress of battery electrodes is a novel approach. Therefore, the measurement principle and the parameters used to assess the drying process are briefly described in this section. Light scattering measurement is a simple method to determine the light scattering properties of a surface. These serve as an important indicator for surface properties such as roughness. Figure 3b illustrates the measurement principle of the scattered light sensor. The light source emits light, which is incident upon the target surface within the measurement range. Some of this light is reflected, with a portion of the reflected light directed towards the lens. The lens guides the light to photodiodes, which are positioned in specific angles, hence, measuring the intensity of the incident light. This process yields the scattered light distribution (Fig. 3a). The characterisation of this distribution involves the use of various statistical parameters. As indicated in the figure, the variance of the scattering angle distribution is denoted as Aq. To minimise statistical deviations, this work employs the mean of multiple measurements (N) in this work:

$$Aqm = \frac{1}{N} \cdot \sum_{n=1}^{N} Aq(n). \tag{1}$$

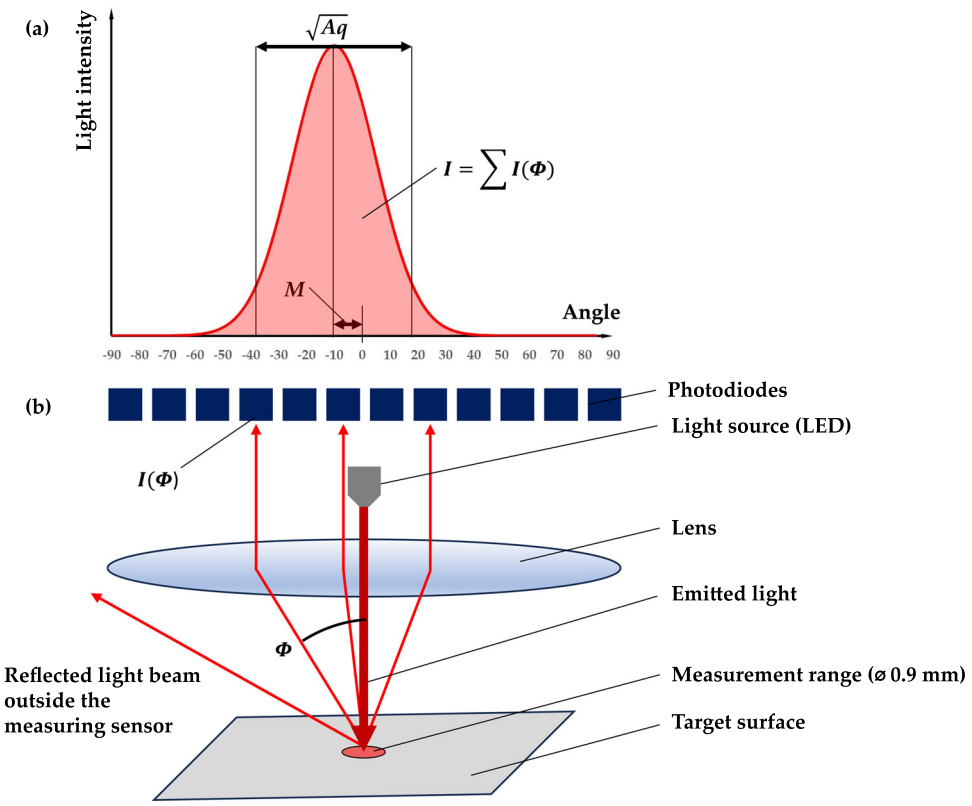

Fig. 3 Schematic representation of the principle of scattered light measurements: **b** The LED light source generates a light beam that is partially reflected on the measurement surface. The lens directs the reflected light onto the photodiodes. The distribution indicated in **a** is obtained by evaluating the light intensities on the individual diodes [22]

Each photodiode detects the light intensity $I(\phi)$ for a specific angle ϕ. The total intensity I is determined by the sum of all diodes. In accordance with the variance Aqm, the mean total intensity Im averaged over N measurements is considered

$$I = \sum I(\phi) \tag{2}$$

$$Im = \frac{1}{N} \cdot \sum_{n=1}^{N} I(n). \tag{3}$$

In this work, a measurement frequency of $f = 30$ Hz has been applied. The mean values Aqm and Im were always calculated for $N = 10$ consecutive measurements. Therefore, one determination of Aqm and Im required a time of $t = 330$ ms. The central position of the angular distribution is denoted by M. This parameter can serve to verify the orthogonal orientation of the sensor to the surface [22].

4 Results and discussion

4.1 Signal evolution during drying process

To demonstrate the capability of the scattered light sensor to detect changes in the electrode surface during drying, initial drying experiments are conducted following the scheme outlined in Sect. 2. Figure 4 (I) shows the temporal evolution of the two characteristic sensor signals, the variance of the scattered light distribution Aqm and the total intensity of the reflected light Im. At the beginning of the drying process, Aqm initially assumes consistently low values, whilst Im remains consistently high, indicating a smooth, reflective surface of the wet electrode layer. During the transition period (approximately 30 s - 55 s), a rapid increase in Aqm and an equally rapid decrease in Im are observed. After about 55 s, this transition period ends, and the values of Aqm reach an upper plateau, where they remain unchanged until the end of the drying process. The values of Im, after the transition period, initially reach a low point and then gradually increase until they reach a constant lower plateau at about 125 s. Apart from this slight, gradual increase observed in the Im curve towards the end of the drying process, apparently the information content of the two parameters Aqm and Im is practically redundant for this application. The characteristic points at which signal changes occur are identical for both parameters. However, it has been observed that the Im value occasionally varies due to thermal influences on the sensor. For these reasons, only the parameter Aqm will be considered for evaluating the progress of drying in further experiments in this study. To detect the progression of the pore emptying, the pore network was observed by digital microscopy during the drying process as described in Sect. 2. The recorded formation of the pore network is shown in Fig. 4 (II). By analysing the video sequence recorded by the microscope, the characteristics of the emptying of the pore network can be illustrated. In the

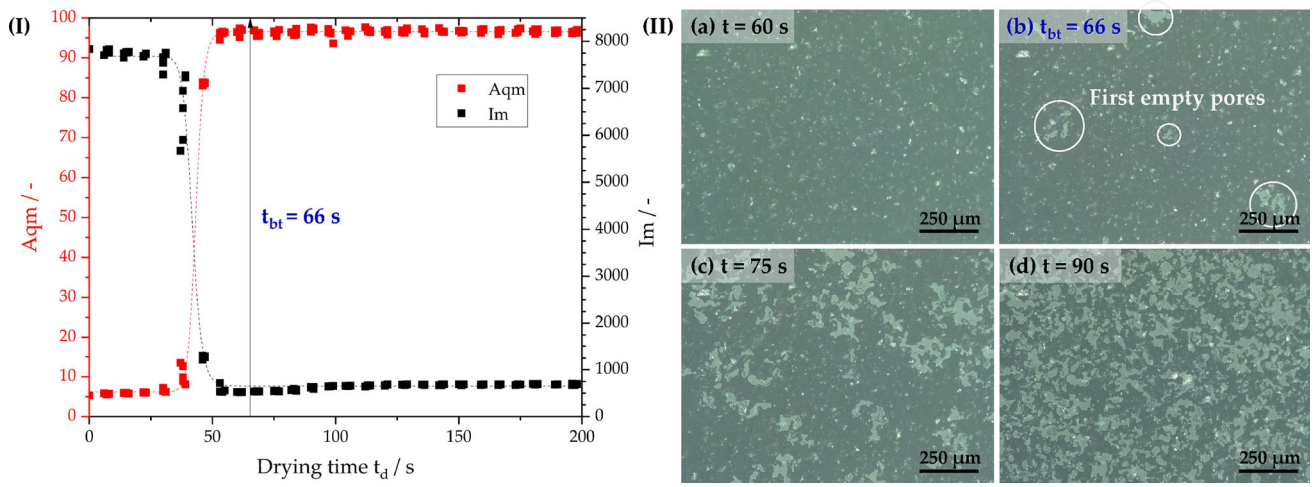

Fig. 4 Detection of the drying progress: (I) Temporal evolution of the parameters Aqm and Im measured by the scattered light sensor during drying compared to the indicated moment of observed pore breakthrough t_{bt}; (II) Progression of the pore emptying recorded from below with a digital microscope; thickness of dry film $d_{dry} = 114$ μm; Heat transfer coefficient $\alpha = 94.5$ W $m^{-2}K^{-1}$; Air temperature $T_{air} = 75$ °C

initial stage of drying (Fig. 4 (II - a), the solvent-filled particle network is visible, and no optical changes can be detected at first. Subsequently, the time of pore breakthrough for the experiment can be accurately determined after 66 s (II - b). Afterwards, the continuous formation of the pore network can be observed until the drying process is complete (II - c,d). As indicated in Fig. 4 (I), the observed pore breakthrough occurs immediately after surpassing the transition region of the sensor signal. This is initially a very plausible observation, considering that the observed pore breakthrough (at the bottom of the layer) occurs slightly delayed in time compared to the onset of pore emptying (at the top of the layer). This simple initial experiment demonstrates the ability of the scattered light sensor to detect the increasing roughness of the electrode surface, evidently caused by the onset of pore emptying, and thus to measure the occurrence of characteristic drying stages. In further, more elaborate experiments, it must now be demonstrated whether the transition point measured by the sensor indeed corresponds to the point at which the drying rate needs to be reduced in a multi-stage drying process according to Jaiser et al. [16] to avoid binder migration.

4.2 Multi-stage drying experiments

A description of the procedure for the conducted transition experiments is provided in Sect. 2. The experiments allow to determine the dependency of the adhesion force of the electrode on the transition time t_{trans} (HDR → LDR). Additionally, measuring the Aqm value at the transition point in each experiment leads to the graphs shown in Fig. 5. A theoretical transition time of $t_{trans} = 0$ s corresponds to the LDR reference sample, whilst a transition time equal to the maximum time required for solvent removal corresponds to the high drying rate (HDR) reference sample.

To ensure that the observed dependencies do not occur only under specific conditions, experiments were conducted with four different parameters ((a) thin layer, (b) medium layer, (c) thick layer, (d) thin layer and increased drying rate). The curves exhibit the same characteristics for all four conditions. For low transition times, both the adhesion forces and the measured Aqm values show a plateau with constant values. Subsequently, there is a rapid increase in Aqm and the expected decrease in adhesion. Across all layer thicknesses and drying rates, it is observed that the point at which adhesion forces decrease coincides with the increasing Aqm values. This confirms the initial hypothesis that the increase in Aqm corresponds to the onset of pore emptying and thus marks the point at which the drying rate should be reduced to prevent binder migration.

It is noticeable that the curves of Aqm and adhesion force exhibit approximate mirror symmetry for medium (b) and high (c) layer thicknesses, with both curves reaching the rear plateau at approximately the same time. Jaiser et al. (2017) defined the attainment of the lower plateau of adhesion forces as the characteristic time point $t_{c,2}$. This represents the moment when drying rates can be increased again without risking binder migration, as the breakdown of capillary network has occurred. Experiments (b) and (c) suggest that this point may also be detected using the scattered light sensor. However, this method is not effective for low layer thicknesses (a), particularly when combined with an increased drying rate (d). Apparently, the formation of higher surface roughness in these cases occurs more abruptly than the decrease in adhesion forces, which lags slightly behind the Aqm curve. Therefore, the scattered light sensor is only capable of detecting the characteristic time point $t_{c,2}$ to a limited extent.

The transition time $t_{c,1}$ for the indicated characteristic is determined by intersecting a tangent drawn to the point of inflection of the logistic curve fit with the upper asymptote, as it has been proposed by Jaiser et al. [16]. For the low layer thickness experimental series (a), a characteristic transition time of $t_{c,1,(a)} = 25$ s is obtained, which is significantly delayed compared to the increase in Aqm and also later than the calculated characteristic time for the experimental series (b) of $t_{c,1,(b)} = 23$ s. However, it is apparent that the adhesion forces in experimental series (a) decrease notably earlier than the calculated $t_{c,1,(a)} = 25$ s. Consequently, the authors emphasise that the methodology proposed by Jaiser et al. [16] is not sufficient to describe the onset of the decrease in adhesion force alone, but it requires a case-by-case consideration. It might be useful to define a different, mathematically more conservative criterion for this purpose in the future.

5 Conclusion

In the present study, the opportunities of the application of a scattered light sensor for monitoring of drying processes of battery electrodes has been explored. Initial experiment demonstrated the sensor's ability to characterise the surface condition of an electrode during the drying process. More elaborated investigations involving multi-stage drying experiments revealed a clear correlation between the increase in the "scattered light" parameter Aqm, which characterises the roughness of the electrode surface, and the decrease in adhesion force for all layer thicknesses and drying rates. Overall, the results provide strong evidence that the scattered light sensor is a useful tool for detecting the onset of pore emptying and thus predicting an optimal transition point during drying. This makes the sensor a valuable tool in two different scenarios: Firstly, for the initial configuration of a dryer.

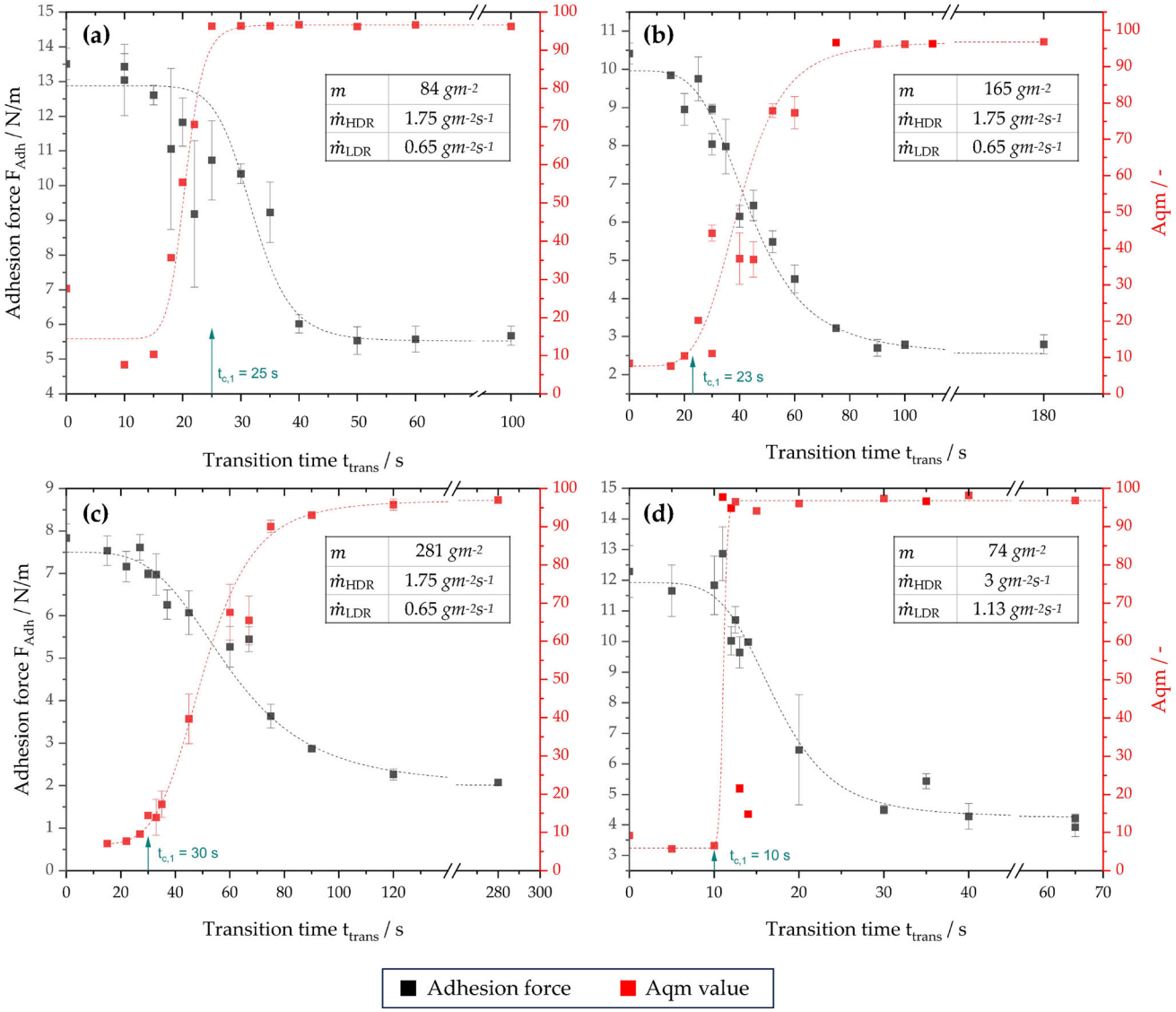

Fig. 5 Dependency of adhesion force of the electrode on the transition time from high drying rate (HDR) to low drying rate (LDR) - compared with the measured *Aqm* value at the transition point. The characteristic transition times $t_{c,1}$ are indicated. The dashed lines represent the logistic fit curves of *Aqm* and adhesion force. **a**–**d** represent different levels of film thickness and drying rates: **a** Low layer thickness (84 gm^{-2}), $\dot{m}_{HDR} = 1.75\ gm^{-2}s^{-1}$, $\dot{m}_{LDR} = 0.65\ gm^{-2}s^{-1}$; **b** Medium layer thickness (165 gm^{-2}), $\dot{m}_{HDR} = 1.75\ gm^{-2}s^{-1}$, $\dot{m}_{LDR} = 0.65\ gm^{-2}s^{-1}$; **c** High layer thickness (281 gm^{-2}), $\dot{m}_{HDR} = 1.75\ gm^{-2}s^{-1}$, $\dot{m}_{LDR} = 0.65\ gm^{-2}s^{-1}$; **d** Low layer thickness (74 gm^{-2}), $\dot{m}_{HDR} = 3\ gm^{-2}s^{-1}$, $\dot{m}_{LDR} = 1.13\ gm^{-2}s^{-1}$

Determining suitable drying rates for each zone is extremely labour-intensive, especially for a three-stage drying process. The sensor can assist in quickly identifying characteristic points and configuring individual dryer zones accordingly. Secondly, the sensor also provides an important opportunity for in-line use during production for the purpose of quality assurance. Deviations from target states, such as premature or delayed onset of pore emptying, can indicate that the electrode is not being dried as intended. The sensor's deployment is feasible due to its simple application, straightforward measuring principle, and robustness against variations in distance caused by vibration within a roll-to-roll setup. Therefore, the use of a scattered light sensor could be a valuable measure to reduce high rejection rates in production.

Acknowledgements The authors would like to acknowledge financial support of the Federal ministry of Education and Research (BMBF) via the AQua cluster-project "IQ-El" (Grant number: FKZ 3XP0359A). This work contributes to the research performed at Center for Electrochemical Energy Storage Ulm-Karlsruhe (CELEST).

Funding Open Access funding enabled and organized by Projekt DEAL.

Data availability The data that support the findings of this study are available from the corresponding author upon reasonable request.

Declarations

Conflict of interest The authors declare no conflict of interest.

References

1. A. Jinasena, O.S. Burheim, A.H. Strømman, A flexible model for benchmarking the energy usage of automotive lithium-ion battery cell manufacturing. Batteries **7**(1), 14 (2021)
2. L. Gaines, Q. Dai, J.T. Vaughey, S. Gillard, Direct recycling r &d at the recell center. Recycling **6**(2), 31 (2021)
3. L. Brückner, J. Frank, T. Elwert, Industrial recycling of lithium-ion batteries—a critical review of metallurgical process routes. Metals **10**(8), 1107 (2020)
4. A. Limé, T. Lein, S. Maletti, K. Schmal, S. Reuber, C. Heubner, A. Michaelis, Impact of electrode defects on battery cell performance: A review. Batteries & Supercaps **5**(10), 202200239 (2022)
5. J. Schnell, G. Reinhart, Quality management for battery production: a quality gate concept. Procedia CIRP **57**, 568–573 (2016)
6. A. Turetskyy, J. Wessel, C. Herrmann, S. Thiede, Data-driven cyber-physical system for quality gates in lithium-ion battery cell manufacturing. Procedia CIRP **93**, 168–173 (2020)
7. J. Kumberg, M. Müller, R. Diehm, S. Spiegel, C. Wachsmann, W. Bauer, P. Scharfer, W. Schabel, Drying of lithium-ion battery anodes for use in high-energy cells: influence of electrode thickness on drying time, adhesion, and crack formation. Energ. Technol. **7**(11), 1900722 (2019)
8. S. Jaiser, M. Müller, M. Baunach, W. Bauer, P. Scharfer, W. Schabel, Investigation of film solidification and binder migration during drying of li-ion battery anodes. J. Power Sources **318**, 210–219 (2016)
9. A. Altvater, T. Heckmann, J.C. Eser, S. Spiegel, P. Scharfer, W. Schabel, (near-) infrared drying of lithium-ion battery electrodes: Influence of energy input on process speed and electrode adhesion. Energ. Technol. **11**(5), 2200785 (2023)
10. F. Font, B. Protas, G. Richardson, J.M. Foster, Binder migration during drying of lithium-ion battery electrodes: Modelling and comparison to experiment. J. Power Sources **393**, 177–185 (2018)
11. M. Baunach, S. Jaiser, S. Schmelzle, H. Nirschl, P. Scharfer, W. Schabel, Delamination behavior of lithium-ion battery anodes: Influence of drying temperature during electrode processing. Drying Technol. **34**(4), 462–473 (2016)
12. Y.S. Zhang, N.E. Courtier, Z. Zhang, K. Liu, J.J. Bailey, A.M. Boyce, G. Richardson, P.R. Shearing, E. Kendrick, D.J. Brett, A review of lithium-ion battery electrode drying: mechanisms and metrology. Adv. Energy Mater. **12**(2), 2102233 (2022)
13. J. Klemens, L. Schneider, E.C. Herbst, N. Bohn, M. Müller, W. Bauer, P. Scharfer, W. Schabel, Drying of ncm cathode electrodes with porous, nanostructured particles versus compact solid particles: comparative study of binder migration as a function of drying conditions. Energ. Technol. **10**(4), 2100985 (2022)
14. J. Klemens, A.-K. Wurba, D. Burger, M. Müller, W. Bauer, S. Büchele, O. Leonet, J.A. Blázquez, I. Boyano, E. Ayerbe et al., Challenges and opportunities for large-scale electrode processing for sodium-ion and lithium-ion battery. Batteries & Supercaps **6**(11), 202300291 (2023)
15. S. Jaiser, L. Funk, M. Baunach, P. Scharfer, W. Schabel, Experimental investigation into battery electrode surfaces: The distribution of liquid at the surface and the emptying of pores during drying. J. Colloid Interface Sci. **494**, 22–31 (2017)
16. S. Jaiser, A. Friske, M. Baunach, P. Scharfer, W. Schabel, Development of a three-stage drying profile based on characteristic drying stages for lithium-ion battery anodes. Drying Technol. **35**(10), 1266–1275 (2017)
17. A. Altvater, J. Klemens, J. Borho, A. Smith, T. Heckmann, P. Scharfer, W. Schabel, Application of multistage drying profiles for accelerated production of li-ion battery anodes using infrared radiation: Validation with electrochemical performance and structural properties. Energy Technology, 2301272 (2024)
18. J. Kumberg, M. Baunach, J.C. Eser, A. Altvater, P. Scharfer, W. Schabel, Influence of layer thickness on the drying of lithium-ion battery electrodes—simulation and experimental validation. Energ. Technol. **9**(5), 2100013 (2021)

19. J. Kumberg, M. Baunach, J.C. Eser, A. Altvater, P. Scharfer, W. Schabel, Investigation of drying curves of lithium-ion battery electrodes with a new gravimetrical double-side batch dryer concept including setup characterization and model simulations. Energ. Technol. **9**(2), 2000889 (2021)
20. A. Finck, Table top system for angle resolved light scattering measurement. Doctoral thesis **318** (2013)
21. M.R. Shenoy, B.P. Pal, B.D. Gupta et al., Design, analysis, and realization of a turbidity sensor based on collection of scattered light by a fiber-optic probe. IEEE Sens. J. **12**(1), 44–50 (2011)
22. Optosurf: Operating Manual: English Version. (2014). Optosurf